

Reducing Car Consumption by Means of a Closed-loop Drag Control

Camila Chovet, Baptiste Plumjeau,
Sebastien Delprat, Marc Lippert
and Laurent Keirsbulck

LAMIH, Umr8201,
59313 Valenciennes, France
email: camila.chovet@univ-valenciennes.fr;
baptiste.plumejeau@icloud.com;
sebastien.delprat@univ-valenciennes.fr;
marc.lippert@univ-valenciennes.fr;
laurent.keirsbulck@univ-valenciennes.fr

Jean-Pierre Richard

Centrale Lille
59651 Villeneuve-d'Ascq, France
email: jean-pierre.richard@centralelille.fr

Maxime Feingesicht
and Andrey Polyakov

INRIA Lille
59651 Villeneuve-d'Ascq, France
email: mfeingesicht@gmail.com;
andrey.polyakov@inria.fr

Franck Kerhervé

Institut P', Upr3346,
86962 Poitiers, France
email: franck.kerherve@univ-poitiers.fr

Abstract—We present a closed-loop separation control experiment on a real car (Renault Twingo GT) using a robust model-based strategy known as Sliding Mode Control (SMC) and whose goal is to decrease the gas consumption through the reduction of the drag force. The study also investigates the feasibility of this control and estimation approach for an industrial framework. A movable spoiler, equipped with slotted air jets, is placed on the top trailing edge of the car in order to actuate the air flow on the rear side of the vehicle. In order to estimate the drag force, the vehicle is instrumented with dSPACE and DEWESoft equipment, which are able to do synchronized measurements in real-time. Concerning the control algorithm, Sliding Mode Control was designed on the basis of a non-linear delayed input-output model, which was recently defined for another flow control application and has shown a good ability for robustness and disturbance rejection.

Keywords—Flow Control; Vehicle; Sliding Mode Control; Drag reduction.

I. INTRODUCTION

In the last years, the sales of automobiles (including cars, trucks, and buses) have sky-rocketed. More than 1 billion vehicles were in operation in 2010 [1]. The amount of transportation automobiles is highly correlated with carbon-dioxide CO₂ emission in the atmosphere, and the strong decrease of oil reserves, to name just a few consequences [2]. Car manufacturers are consequently urged to develop new technologies, which can contribute to significantly diminish the environmental impact of transportation [3]. In this regard, four development areas are identified to improve energy consumption, autonomy and gas emissions: engine performance, reduced friction of the bearings, the lightening of the mass of the vehicle and the aerodynamics [1]. The work in progress presented in this article targets the latter one. The power consumed to resist the drag constitutes an important portion of the total power expense. For example, the aerodynamic drag of a car, at a speed of 50 km/h, accounts for 50 % of the total drag, reaching 80 % at 130 km/h [4]. Initially, drag reduction was achieved through vehicle shape. This explains why most of the present cars have similar enclosures [5]; vehicles tend to follow a unique shape in order to optimize drag reduction. Nonetheless,

there is room to further reduce the aerodynamic drag thanks to the manipulation and/or control of the wake flow. This approach is of great challenge for the transport industry and must be tackled as a multidisciplinary field. A combination of passive and active devices might decrease the drag force by enhancing the shear layer deflection [6]. Our aim is to tackle this industrial problematic through the knowledge of different academic areas.

The main goal is to develop an effective control strategy combined with an industrial actuator to minimize the drag of a real car and thus reduce both fuel consumption and gas emissions.

The paper is organized into three sections: Section II presents the instrumented vehicle. Section III is devoted in estimating the drag force for a real car configuration, while Section IV briefly defines the design of the closed-loop strategy on an Ahmed body configuration. It will be shown how Sliding Mode Control is able to reduce and maintain the drag to a desired set-point regardless of external flow perturbations. A short conclusion and perspectives are presented in Section V.

II. INSTRUMENTED VEHICLE

The instrumented vehicle used for experiment proposes is a Renault Twingo II C44 GT owned by LAMIH laboratory. The dimensions of the car are as follows: height H of 1.47 m (from the top part of the car to the floor), width $w=1.39$ m and, length $l=3.69$ m (see Fig.1(a) and Fig.1(b)). Due to the presence of two people inside the vehicle, it has two different ground clearances. The first one closer to the front wheel $g_1=38.6$ cm, while the second is measured at the back wheel and is equal to $g_2=51$ cm. The results presented are for car velocities from 45 km/h to 130 km/h, which correspond to Reynolds numbers, based on the car height $h \approx 1.02$ ($h = H - (g_1 + g_2)/2$), of $Re_h \approx 6 \times 10^6 - 19 \times 10^6$. The results will be described in a Cartesian coordinate system x , y and z representing the stream-, transverse- (normal to ground) and span-wise directions, respectively (see Fig.1(a) and Fig.1(c)). Experiments will take place on a 2km race track

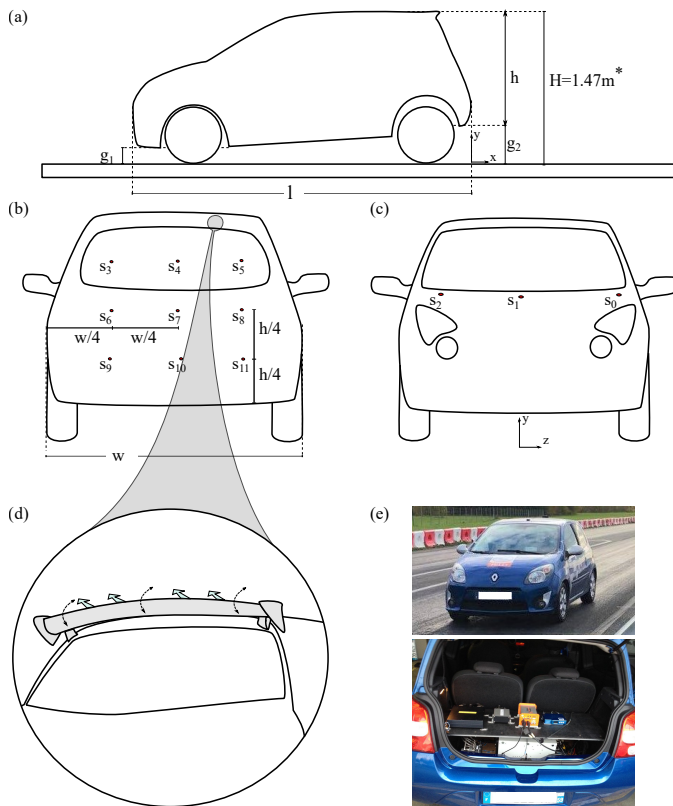


Figure 1. Sketch of the vehicle Twingo GT. (a) Rear view, (b) Front view, (c) Actuation mechanism, (d) Side view, (e) Real vehicle image.

located at Clastres (North of France). The track is travelled in both directions, direction I (dI): departure to arrival and direction II (dII): arrival to departure.

The car is equipped with a GPS, which is able to measure the longitude and latitude coordinates (x and z directions, respectively). The slope of the road is retrieved from GPS measurements. GPS data is projected on a local plane (Lambert Projection 93), and the $x - z$ data is then projected on a local coordinate system aligned with the track and centred at the end of the runway. The z -coordinate measures the lateral deviation from the reference axis. Furthermore, the car is also equipped with two acquisition systems: DEWESoft and dSPACE. Since two measurement devices are used, the data must be re-calibrated. For this, a binary signal is sent from dSPACE to DEWESoft. The registration is then carried out by synchronizing the first rising edge. Twelve sub-miniature piezo-resistive Kulite XCQ-0.62 sensors are placed at the front and the back of the car. Three of them are placed at the front close to the windshield, the first one is located at the center plane $w/2$ from the side of the body while the other two are at distance $w/8$ from the car side edge (one at each side). On the rear, 9 pressure sensors were also set. The distance between each sensor is $y = h/4$ and $x = w/4$ starting at the same $x - y$ distance, for a clear view of the sensor positions please refer to Fig.1(b) and Fig.1(c). Finally, an innovative actuation mechanism will be placed at the top trailing edge of the vehicle (see Fig.1(d)). A movable spoiler (commercially available) will be equipped with slotted jets in order to vary key actuation parameters such as angle, pressure (jet velocity), DC (Duty cycle) and frequency.

III. FORCE ESTIMATION

In order to estimate the drag force, two mechanisms are here presented. The first one is with an approximation of Onorato relation [7]. 80% of the total drag force is related to the pressure forces. From this statement, the integral balance of momentum is simplified as:

$$F_x = \iint_{S_w} (Pt^\infty - Pt^{S_w}) d\sigma \quad (1)$$

where S_w denotes the surface of the wake downstream the vehicle, Pt^∞ and Pt^{S_w} are the upstream pressure and the pressure in the wake S_w . With this equation, the drag coefficient C_x can be calculated from equation presented by Onorato [8]. Taking into account the twelve pressure probes placed in the car, and an equal area for all the sensors, the drag coefficient can be approximated as

$$C_x \approx \frac{\sum_{n=1}^3 (Pt_n^\infty) - \sum_{n=1}^9 (Pt_n^{S_w})}{1/2\rho U_\infty^2} \quad (2)$$

The second one is through an estimation of the external forces presented in the car. Once a portion of the data is selected, it is now possible to estimate the external forces exerted on the vehicle. The dynamics of the vehicle is expressed in the form of an energy balance equation:

$$M \frac{dv(t)}{dt} = F_{mot}(t) \pm mgsin(\vartheta(d(t))) - F_{ext}(t) \quad (3)$$

The longitudinal acceleration $\frac{dv(t)}{dt}$ is obtained through the central inertial unit, while the slope ϑ was previously measured using the average slope measurement as a function of the distance $d(t)$ travelled. The \pm sign in equation.3 is related to the fact that the track is travelled in both directions. In the direction I, the vehicle undergoes a headwind and a slight rise. In direction II, the vehicle undergoes a wind of back and a slight descent. The estimation of the external force $F_{ext}(t)$ is trivial via (3). Additionally, the external force is decomposed as follows:

$$F_{ext}(t) = C_{rr}mgcos(\pm\vartheta) + 1/2\rho AfC_d(v(t) \pm v_{wind})^2 \quad (4)$$
 with v_{wind} the unknown wind velocity assumed constant. For simplification, $\alpha_1 = C_{rr}mgcos(\pm\vartheta)$ and $\alpha_2 = 1/2\rho AfC_d$. In (3) the term $cos(\pm\vartheta)$ is assumed constant because of the co-sinus function is even, so the sign of the slope will not influence the results. Each test is thus summarized to a pair $(\bar{v}(i), F_{ext}^- (i))$. Then, the parameters are estimated by minimizing a quadratic model error:

$$J = \sum_{i.e.dI} (F_{ext}^- (i) - \alpha_1 - \alpha_2(\bar{v}(i) - v_{wind})^2)^2 + \sum_{i.e.dII} (F_{ext}^- (i) - \alpha_1 - \alpha_2(\bar{v}(i) + v_{wind})^2)^2$$

The minimization of J , starting from a realistic solution, relates to an optimization problem and leads to solving a linear problem for α_1 and α_2 , which can be solved in a straightforward manner. The introduction of wind speed complicates the calculation of the solution and a Trust-Region Quasi-Newton algorithm is necessary.

The drag coefficient C_x is presented in Fig.2 for a velocity range of $U_\infty \in [45 \text{ km/h}, 130 \text{ km/h}]$ calculated from the

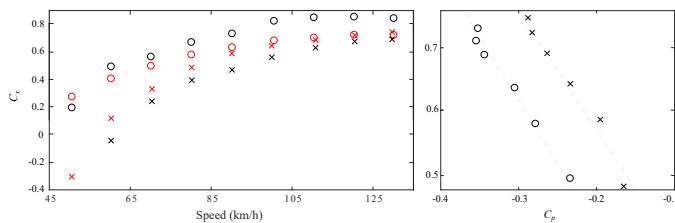


Figure 2. (a) C_x obtained for different velocities using the two approaches. (b) Relation between C_x and C_p .

two estimation approaches (red symbols: results using estimation approach, black symbols: results using Onorato's drag approximation). The figure shows both direction results. A positive curved increase of the C_x is present for an increase in the velocity. Similar results are obtained for both approaches, which means there is a good estimation of the drag force. A small gap is seen from the results in direction I (departure to arrival, circle symbols) and direction II (arrival to departure, times symbol). This is due to the effects of the wind that clearly induced some variations in the results depending on which direction the track is run. The ratio between the C_p obtained from the pressure sensor and the C_x estimated from the energy balance is presented in Fig.2(b). A linear relation is obtained, for both directions. It is possible to conclude that both methodologies could be used as sensors to estimate the drag of a real car. It is worth noting that external parameters, such as wind speed, probably varied and therefore errors are introduced in the measures.

IV. EXPERIMENTAL RESULTS OF SMC APPLICATION

As previously stated, the goal is to reduce and further maintain the aerodynamic drag of a square-back Ahmed regardless of incoming flow perturbations or again measurement noise and model inaccuracies. To achieve this, we consider the first closed-loop separation control experiment on a simplified car model, also known as Ahmed body, using a robust, model-based strategy called Sliding Mode Control. This control approach is based on an initial black-box model identification presented by Feingesicht et al. (2016 & 2017) [9][10]. Without loss of generality, the sliding mode principle is a problem of a set-point tracking where a control system is considered as the form,

$$\dot{s}(t) = f(s, t) + g(s, t)b(t) \quad (5)$$

where f and g are unknown functions and $b(t) \in \{0, 1\}$ is the relay control input, s is the state and t is the time. The objective is to determine a control that guarantees $s(t) \rightarrow s^*$ as $t \rightarrow +\infty$, where s^* is a desired set-point. The control must be also robust with respect to some uncertainties in f and g . If we can force the dynamics of the system to lie on a well behaved surface, then the control problem is greatly simplified. Sliding Mode Control [11] is based on the design of an adequate "sliding surface" (or "sliding manifold") defined as,

$$\Sigma = \{(s, t) \mid \sigma(s, t) = 0\} \quad (6)$$

that divides the state space into two parts, which correspond to one of the two controls, which commute between two pre-defined values (typically zero and one or +V and -V for a relay) when the state crosses the surface in order to maintain the sliding mode $\sigma(s(t), t) = 0$. The manifold Σ is defined in

such a way that the error $|s(t) - s^*|$ vanishes to zero when the system state s is restricted to lie on this surface. The control problem then reduces to the problem of reaching phase during which trajectories starting off the manifold Σ move toward it in a finite time, followed by a sliding phase during which the motion is confined to the manifold and the dynamics of the system are represented by the reduced-order model.

An identification procedure of the dynamical system is employed here for flow control application. In the present case, the sensor output utilized is the instantaneous drag $F_D(t)$, the control variable $s(t) = F_D^\infty - F_D(t)$, where F_D^∞ is a drag in the uncontrolled steady state, and the control command is the switching function $b(t)$ send to the actuators. Due to the non-linear nature of the governing equations driven the flow dynamics, non-linear models with time-delays are here preferred. The bilinear model proposed by Feingesicht et al. (2016 & 2017) [9], [10] is here considered and can be written as,

$$\dot{s}(t) = \alpha_1 s(t-h) - \alpha_2 s(t) + (\beta - \gamma s(t-h) + \gamma s(t-\tau))b(t-h) \quad (7)$$

where α_i , β , γ , h and τ are positive constant parameters to identify. Identification of the model parameters is performed thanks to open-loop control experiments, which consists in successive cycles of actuation and relaxation phases for different values of the control parameters (here frequency F_A and duty-cycle DC). For conciseness, the reader is referred Feingesicht et al. (2017) [10] for full details of the identification procedure. In the present case, it leads to $\alpha_1 = 27.37$, $\alpha_2 = 32.70$, $\beta = 1.97$, $\gamma = 1.92$, $\tau = 0.18$ s and $h = 0.01$ s. The precision of the model has been evaluated by a FIT index, presented by Choivet et al. [12] equal to 59% for the present application.

Experiments were conducted in a closed-loop wind tunnel (2 m wide, 2 m high and 10 m long). The blunt-edged bluff body is a simplified car model known as square-back Ahmed body, Fig.3(a), with the following dimensions: height $h=0.135$ m, width $w=0.170$ m and length $l=0.370$ m. The model was mounted over a raised floor with a ground clearance of $g=0.035$ m. The Reynolds number was kept constant at $Re_h = 9.10^4$. Based on previous open-loop results, the set-point $s^* = -2.5\%$ is considered as the tracked value. Drag force was measured using a 6-components DELTA-ATI aerodynamic balance. The velocity flow fields were obtained using a standard two-component TSI Particle Image Velocimetry (PIV) system. The system consists of a double-pulse laser system generating the light sheet and two cameras recording the light scattered by the tracer particles. The model is equipped with an actuator slit at the top trailing edge. The slit width is $h_s = 0.5$ mm and the actuation length is $w_a = 150$ mm. The pressured air, supplied by a compressed air reservoir, can be blown tangentially to the free-stream velocity through the slit (see Fig.3(b)). The pulsed blowing is driven by a FESTO-MH2 solenoid valve that can generate an on/off pulsed jet within an actuation frequency range between $f_A = 0 - 500$ Hz. A rounded surface, adjacent to the slit exit, with an additional plate is installed to blow the jet in a predefined direction (for this case we used an actuation an $\theta = -6^\circ$, shown in Fig.3(c)). We choose a pressure value of $P_a = 6$ bars and a forcing frequency control DC of 50%, giving a maximum jet velocity of 32.2 m/s. The real-time processing was achieved using an Arduino board, with a sampling rate fixed at 100 Hz.

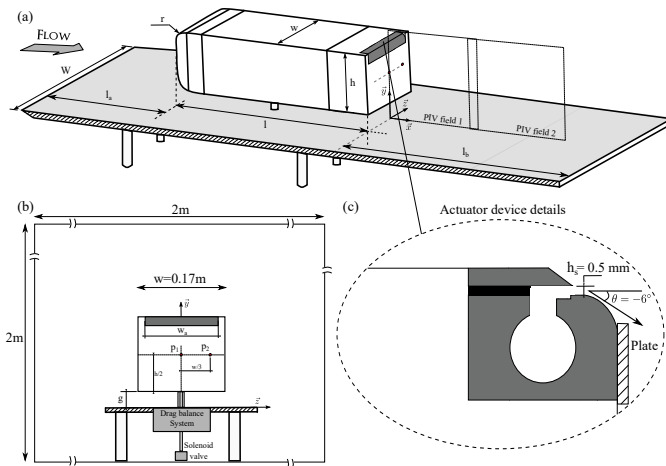


Figure 3. Ahmed body setup

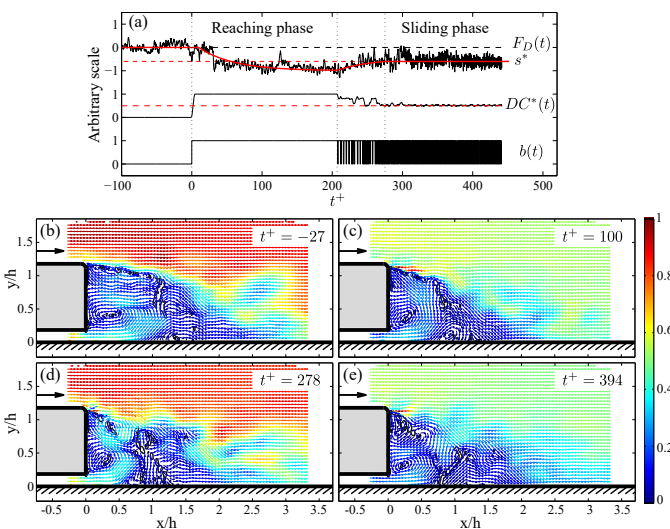


Figure 4. SMC set-point tracking results: upper plot shows the time history response. Instantaneous flow field captured by the PIV for several forced configurations.

An overview of the results obtained with the SMC is shown in Figures 4, for a further analysis of the wake dynamics please refer to [12]. Figure 4.a shows the time response of the drag (top line) for the forcing command $b(t)$ when the closed-loop controller is activated (bottom line). The calculated instantaneous duty-cycle DC^* , presented in [12], is also reported in this figure (middle line). Snapshots at four distinct instants of these time histories are reported in Figures 4.b-e. Three distinct control phases are noticeable in Figures 4.a. When the actuation is activated ($t^+ = 0$), the controller enters a phase known as “reaching phase” whose objective is to approach rapidly the targeted set-point and during which the drag force is found to decrease rapidly. In the present case, this phase corresponds to a steady blowing forcing as seen in Figures 4.a where the DC^* is found equal to unity. A transition phase ($200 < t^+ < 280$) is then observed during which the controller seeks the adequate ON-OFF combination to rapidly reach the targeted set-point. Finally, the last phase ($t^+ > 280$) corresponds to the so-called “sliding phase” where the controller attempts to maintain the drag at the tracked value s^* despite any disturbances on the plant.

V. CONCLUSION

The propositions presented in this short paper may be used as a reference to orient the work of flow control towards drag reduction. The ideas proposed here are a consequence of all the work done for simpler configurations. Their use in an industrial application or as an ‘experimental showcase’ is of great promise in future works. The car characteristics, equipment, and actuator are presented in Section II, the vehicle is already equipped with apparatus able to do measurements such as pressure, position, etc. Furthermore, a movable spoiler with jets will be added in order to control the rear wake. To achieve closed-loop control, two approaches are proposed in Section III. The first one is an approximation of Onorato’s equation while the second one is an estimation of the drag force through external forces equation. Similar drag coefficients C_x were obtained for both propositions. The initial results in this experience present the possibility to directly estimate the drag of a car. Finally, we present a novel, robust closed-loop control to reduce and maintain the drag. We are interested in steering the drag of an Ahmed body to a set-point s^* and stabilizing it regardless of external conditions. In principle, the control approach can be seen as a compilation of open-loop control tests. However, the actuation frequency has to be selected carefully in real-time depending on the external parameters up- and down-stream of the flow. Otherwise, actuation energy is wasted. The robustness and easy implementation in an experimental set-up make this approach convenient for industrial applications. Also, SMC might be able to take into account model design errors of drag estimation, keeping the drag at a certain value, regardless of these errors. Hence, the benefits of SMC can be fully exploited.

ACKNOWLEDGMENT

This work is being held within the framework of the CNRS Research Federation on Ground Transports and Mobility, in articulation with the ELSAT2020 project supported by the European Community, the French Ministry of Higher Education and Research, the Hauts de France Regional Council. The authors gratefully acknowledge the support of these institutions. The authors declare that they have no conflict of interest.

REFERENCES

- [1] R. Li, “Aerodynamic drag reduction of a square-back car model using linear genetic programming and physics-based control”. PhD. thesis, Pprime, Poitiers, France, 2017.
- [2] D. Sperling and D. Gordon, “Two billion cars: transforming a culture”. *TR news* 259., 2008.
- [3] W.-H. Hucho, “Aerodynamics of road vehicles”. *Society of Automotive Engineers*, e.d. 1998.
- [4] S. L. Brunton, and B. R. Noack, “Closed-loop turbulence control: Progress and challenges”. *Appl. Mech. Rev.* 67(5), 050801, pp.01-48, 2015.
- [5] G. Rossitto, “Influence of afterbody rounding on the aerodynamics of a fastback vehicle”. PhD. thesis, École Nationale Supérieure de Mécanique et d’Aérotechnique, Poitiers, France, 2016.
- [6] R. J. Englar, “Pneumatic heavy vehicle aerodynamic drag reduction, safety enhancement, and performance improvement”. *The Aerodynamics of Heavy Vehicles: Trucks, Buses, and Trains*, pp. 277-302, Springer, 2004.
- [7] M. Onorato, A. F. Costelli and A. Garonne, “Drag measurement through wake analysis”. *SAE, SP-569, International congress and Exposition*, Detroit, MI, pp. 85-93, 1984.
- [8] Y. Eulalie, “Aerodynamic analysis and drag reduction around an Ahmed bluff body”. PhD. thesis, Bordeaux Univ, 2014.

- [9] M. Feingessicht, C. Raibaud, A. Polyakov, F. Kerhervé and J. -P. Richard, "A bilinear input-output model with state-dependent delay for separated flow control". *European Control Conference*, pp. Aalborg, Denmark, 2016.
- [10] M. Feingessicht, A. Polyakov, F. Kerhervé and J. -P. Richard, "SISO model-based control of separated flows: Sliding mode and optimal control approaches". *Int. J. Robust and Nonlinear Control*, 27(18), pp. 5008-5027, 2017, DOI:10.1002/rnc.3843.
- [11] V. Utkin, "Sliding Modes in Control Optimization". *CCES Springer-Verlag*, Berlin, 1991.
- [12] C. Chovet et al., "Sliding mode control applied to a square-back ahmed body". *J. Fluid Mech.*, 2018b (Under revision).